

Sensitive surface loop-gap microresonators for electron spin resonance

Ygal Twig, Ekaterina Suhovoy, and Aharon Blank

Citation: *Rev. Sci. Instrum.* **81**, 104703 (2010); doi: 10.1063/1.3488365

View online: <http://dx.doi.org/10.1063/1.3488365>

View Table of Contents: <http://rsi.aip.org/resource/1/RSINAK/v81/i10>

Published by the [American Institute of Physics](#).

Related Articles

Electrical transduction in nanomechanical resonators based on doubly clamped bottom-up silicon nanowires
Appl. Phys. Lett. **101**, 243115 (2012)

Strongly coupled modes in a weakly driven micromechanical resonator
Appl. Phys. Lett. **101**, 243111 (2012)

Experimental characterisation of a novel viscoelastic rectifier design
Biomechanics **6**, 044112 (2012)

Focused ion beam milling and deposition techniques in validation of mass change value and position determination method for micro and nanomechanical sensors
J. Appl. Phys. **112**, 114509 (2012)

Analyzing threshold pressure limitations in microfluidic transistors for self-regulated microfluidic circuits
Appl. Phys. Lett. **101**, 234107 (2012)

Additional information on *Rev. Sci. Instrum.*

Journal Homepage: <http://rsi.aip.org>


Journal Information: http://rsi.aip.org/about/about_the_journal

Top downloads: http://rsi.aip.org/features/most_downloaded

Information for Authors: <http://rsi.aip.org/authors>

ADVERTISEMENT

JANIS Does your research require low temperatures? Contact Janis today.
Our engineers will assist you in choosing the best system for your application.



10 mK to 800 K **LHe/LN₂ Cryostats**
Cryocoolers **Magnet Systems**
Dilution Refrigerator Systems
Micro-manipulated Probe Stations

sales@janis.com **www.janis.com**
Click to view our product web page.

Sensitive surface loop-gap microresonators for electron spin resonance

Ygal Twig, Ekaterina Suhovoy, and Aharon Blank^{a)}

Schulich Faculty of Chemistry, Technion-Israel Institute of Technology, Haifa 32000, Israel

(Received 6 July 2010; accepted 18 August 2010; published online 21 October 2010)

This work presents the design, construction, and experimental testing of unique sensitive surface loop-gap microresonators for electron spin resonance (ESR) measurements. These resonators are made of “U”-shaped gold structures with typical sizes of 50 and 150 μm that are deposited on a thin (220 μm) rutile substrate and fed from the rear by a microstrip line. This allows accommodating a large flat sample above the resonator in addition to having variable coupling properties. Such resonators have a very small volume which, compared to previous designs, improves their absolute spin sensitivity by a factor of more than 2 (based on experimental results). They also have a very high microwave field-power conversion ratio of up to 86 gauss/ $\sqrt{\text{Hz}}$. This could facilitate the use of very short excitation pulses with relatively low microwave power. Following the presentation and the discussion of the experimental results, ways to further increase sensitivity significantly are outlined. © 2010 American Institute of Physics.

[doi:10.1063/1.3488365]

I. INTRODUCTION

Electron spin resonance (ESR) is a powerful spectroscopic method employed in the study of free radicals, crystal defects, and transient paramagnetic species. ESR is used extensively in fields of science ranging from physics to biology and from medicine to materials science. One of the most severe limitations of ESR is its relative low sensitivity, compared to other spectroscopic techniques (e.g., fluorescence or mass spectroscopy). This is mainly due to the low energy gap between the magnetic field ESR transitions observed during the ESR experiment. Modern conventional ESR spectrometers use induction (Faraday) detection with a high quality (Q -factor) rectangular cavity, which enables a typical sensitivity of $\sim 10^9$ spins/ $\sqrt{\text{Hz}}$.¹ This limited capability led to the development of novel ultrasensitive detection methods such as magnetic resonance force microscopy,^{2,3} scanning tunneling microscopy combined with ESR (STM-ESR),^{4–6} and indirect optical detection via nitrogen-vacancy center in diamond.^{7,8} However, these new methods suffer from a variety of problems, such as poor spectroscopic capabilities, complex samples preparation, limited field of view, and other issues (see Ref. 9 for more details) that limit their practical use. Currently there is no commercial system that can employ any of these new techniques. As a result, the need for high sensitivity *induction-detection-based* systems is still very strong and one must keep looking into methods for greatly improving the sensitivity of the conventional ESR detection scheme. At the heart of any conventional ESR system lies the microwave resonator, whose properties can determine the ultimate system performance. Here we present the design, construction method, and experimental testing of

a new family of surface loop-gap microresonators with variable coupling capabilities that can greatly improve the spin sensitivity of conventional ESR systems, based on induction-detection. Such resonators can be useful for a variety of application such as detection and imaging of defects on the surface and subsurface of semiconductors,^{10,11} measurements of paramagnetic monolayers,¹² inspection of small biological systems, such as single cells internalized by stable radicals or paramagnetic labeled membranes,¹³ and, in general, performing ESR spectroscopic measurements on spin-limited samples.

II. THE SENSITIVITY OF INDUCTION-DETECTION ESR

Induction-detection ESR experiments can be carried out in continuous-wave (cw) or in pulsed mode. The former can be applied to all types of samples, but with lower spectroscopic versatility and smaller sensitivity per entire spectrum acquisition; while the latter is more versatile and sensitive, but applicable only to samples with a relatively long spin-spin relaxation time, T_2 . Furthermore, pulsed ESR is difficult to apply with resonators having a very high Q -factor. The sensitivity of both cw and pulsed methods is equally dependent on typical sample and resonator characteristics, up to a constant.^{9,14,15} Thus, although the present theoretical and experimental work is conducted in conjunction with pulsed mode instrumentation, the parametric sensitivity behavior is relevant also to cw mode. The single-shot signal-to-noise-ratio (SNR) of a small sample with a volume V_v (e.g., a single voxel of an ESR image out of a larger sample) in a pulsed ESR experiment is given by the expression^{9,14}

$$\text{SNR}_{\text{pulse}}^{\text{single shot}} \approx \frac{M\omega_0 V_v}{4\sqrt{k_b T \Delta f}} C_p, \quad (1)$$

where M is the specific net magnetization of the sample (units of $[\text{J T}^{-1} \text{m}^{-3}]$), as given by the Curie law,¹⁶ ω_0 is the

^{a)} Author to whom correspondence should be addressed. Telephone: +972-4-829-3679. Fax: +972-4-829-5948. Electronic mail: ab359@tx.technion.ac.il.

Larmor angular frequency, k_b is the Boltzmann constant, T is the temperature in which the experiment is carried out (assumed to be the same for the spins and the resonator), and Δf is the bandwidth of signal acquisition. Equation (1) assumes that the noise is four times larger than the theoretical lower limit (for a dominant Johnson noise source). The factor C_p is the resonator's field-power conversion ratio, i.e., the amplitude of the B_1 field in the resonator produced by 1 W of excitation microwave power, which is given by the expression (for a critically coupled resonator)¹⁷

$$C_p \approx \sqrt{Q_u \mu_0 / 2V_c \omega_0}. \quad (2)$$

Here, μ_0 is the free-space permeability and Q_u is the unloaded quality factor of the resonator. The symbol V_c represents the resonator's effective volume, which is equal to the volume of a small hypothetical sample V_v (for example $[1 \mu\text{m}]^3$, usually located at the point where the resonator's microwave magnetic field is maximal), divided by the filling factor¹⁷ of this small sample.¹⁴

There is a fine but important point that should be emphasized with respect to C_p . As we shall see below, there are resonators in which the B_1 microwave field can have very large spatial variations within the resonator (in areas where the sample is placed). This, in principle, means that C_p can vary significantly for different locations in the resonator volume. To account for that we can define C_p in a more general manner, in which we consider V_c not as a single value for the resonator but rather as a variable, depending on which V_v we choose inside the resonator. Thus, for example, if V_v is located at the strongest B_1 field point in the resonator, its corresponding V_c (according to the definition above) will be the smallest and C_p will be the largest. However, if V_v is located at a relatively weak area of B_1 in the resonator, then its V_c will be relatively large and C_p will be small. We shall use this notion of a position-specific C_p in our discussion below.

Equation (1) can be combined with Eq. (2) to obtain the expression⁹

$$\text{SNR}_{\text{pulse}}^{\text{single shot}} \approx \frac{\sqrt{2\mu_0 M \omega_0 V_v}}{8\sqrt{V_c} \sqrt{k_b T \Delta f}} \sqrt{\frac{Q_u}{\omega_0}}. \quad (3)$$

Therefore, for an acquisition time of one second we can get a SNR of

$$\text{SNR}_{\text{pulse}}^{\text{one second}} \approx \frac{\sqrt{2\mu_0 M \omega_0 V_v}}{8\sqrt{V_c} \sqrt{k_b T (1/\pi T_2^*)}} \sqrt{\frac{Q_u}{\omega_0}} \sqrt{\frac{1}{T_1}}. \quad (4)$$

Here we assumed an averaging with a repetition rate equal to $1/T_1$ for SNR improvement and that the chosen excitation bandwidth matches the linewidth of the imaged paramagnetic species in the sample, $\Delta f = 1/\pi T_2^*$. The result of Eq. (4) can be converted into sensitivity expressed by the minimal number of detectable spins/ $\sqrt{\text{Hz}}$ by assuming $\text{SNR}=1$ and knowing that $MV_v B_F / \mu_B$ is the number of spins in our small sample

$$\begin{aligned} \frac{MV_v B_F}{\mu_B} &= \text{sensitivity}_{\sqrt{\text{Hz}}}^{\text{spins}} \\ &\approx \frac{8\sqrt{V_c} \sqrt{k_b T (1/\pi T_2^*)}}{\mu_B \omega_0 \sqrt{2\mu_0}} \sqrt{\frac{\omega_0}{Q_u}} \sqrt{T_1 B_F}, \end{aligned} \quad (5)$$

where B_F is the Boltzmann population factor

$$B_F = \frac{1 + e^{-\hbar\omega_0/k_B T}}{1 - e^{-\hbar\omega_0/k_B T}}$$

and μ_B is Bohr's magneton.

In cw ESR, sensitivity is often reported as spins/gauss $\sqrt{\text{Hz}}$, which provides the minimal detectable number of spins of a sample with a linewidth of 1 gauss that does not saturate. For such samples, cw sensitivity expressed in spins/gauss $\sqrt{\text{Hz}}$ would be very similar to the value of the pulsed-operation sensitivity expressed in spins/ $\sqrt{\text{Hz}}$. For other types of samples and when one does consider saturation conditions, the comparison is more complicated as other factors come into play (available power, modulation amplitude, etc.). However, as noted above, if we assume optimal power and modulation conditions, we can also express cw sensitivity in spins/ $\sqrt{\text{Hz}}$ and then find that the SNR general functional dependence on system parameters is similar for both cw and pulsed ESR.^{14,15}

It is clear from Eq. (5) that if the sample of interest is much smaller than V_c (as in the case of single spin detection or in imaging experiments, where V_v is a typical small voxel size), it would be better to reduce the size of the resonator and thereby increase its absolute spin sensitivity. [However, it should be kept in mind that for an unlimited sample volume (i.e., when $V_v \sim V_c$) it is better to increase the resonator's size to improve spin *concentration* sensitivity.] This philosophy regarding the decrease in resonator size has guided our recent work with dielectric resonators, where we employed high-permittivity single-crystals leading to a relatively small V_c of $\sim 1 \text{ mm}^3$ at 17 GHz. Such type of resonator (with $Q_u=1000$) enables a theoretical spin sensitivity of $\sim 5.3 \times 10^7$ spins/ $\sqrt{\text{Hz}}$ [according to Eq. (5)], which was verified in an imaging experiment (using a LiPc sample having $T_1=3.5 \mu\text{s}$ and $T_2=2.5 \mu\text{s}$).⁹

All of the above indeed shows the clear advantages of reducing the resonator's dimensions. Still, there is a limit to the possible size reduction of dielectric resonators. For any given resonance frequency, the size of the dielectric resonator decreases as the permittivity of its material increases (linear dimensions proportional to $1/\sqrt{\epsilon}$, see Ref. 9). However, the upper limit of available permittivity values in both natural and man-made materials is a few hundreds.¹⁸ A possible way around this problem is to examine metallic or combined metallic/dielectric structures. These can be made resonant in a variety of sizes, with the possibility of typical dimensions reaching values that are much smaller than the wavelength of the microwave irradiation. In order to increase spin sensitivity, ideally the resonators should have low dimensionality [e.g., quasi-two-dimensional (2D) or -one-dimensional (1D)], to further reduce their volume. For example, Narkowicz and co-workers have recently pursued this direction by designing and constructing planar microresonators with a di-

ameter as small as $20\ \mu\text{m}$ and resonance frequency of $\sim 14\ \text{GHz}$.^{19,20} Other microstrip-based ESR surface resonators that are half-wavelength long and have a somewhat simpler design but are larger in size have also been described.²¹ The small V_c of this type of structures enables them to achieve very high spin sensitivity, even though their Q -factor may be relatively low. In their work, Narkowicz and his co-workers calculated that a $20\text{-}\mu\text{m}$ -diameter resonator, which is used to measure a DPPH sample with $\sim 2\text{-G}$ linewidth in CW mode, can provide a minimal detectable number of $\sim 2 \times 10^8$ spins/ $\sqrt{\text{Hz}}$. Their experimentally measured value was found to be $\sim 10^9$ spins/ $\sqrt{\text{Hz}}$. These sensitivity values should more or less be the same for the sample we used in our imaging work (LiPc crystals), since both materials have a T_2 ($\sim T_2^*$) that is almost equal to T_1 and thus the ratio of T_1/T_2^* that comes into play in the spin sensitivity Eq. (5) [and also in Eq. (3) in Narcotic's paper]¹⁹ would not change much. These sensitivity values come very close to the ones we obtained using dielectric resonators that are larger in size but have a much higher Q -factor.⁹

Such types of planar resonator configuration are very promising but have some limitations. The first is their low Q -factor (around 15 for the small resonators); the second is the lack of convenient variable coupling capabilities that are important to accommodate different types of samples, and/or to compensate for varying resonator properties at different temperatures. A third problem is related to the second one, namely, that the coupling tuning/matching is based on fixed microstrip patches that tend to be much larger than the resonator. This leads to the microwave magnetic field spreading out to many parts of the resonator assembly and especially along the coupling tuning/matching patches,^{19,20} which increases the effective volume of the resonator (V_c) and thus reduces its overall sensitivity. Here we present the design, construction method, and testing of a new family of surface microresonators that we denote "surface loop-gap microresonators" with variable coupling capabilities. The design provides flexibility for accommodating a variety of samples without affecting resonator matching. Furthermore, the microwave magnetic fields are confined only to the resonator's structure, leading to a very small V_c and therefore to improved spin sensitivity.

III. SURFACE LOOP-GAP MICRORESONATORS

Planar printed resonators are common in microwave circuitry and are used, for example, as the basis of filters,²² oscillators,²³ and as a basis for metamaterials with negative permittivity and permeability.²⁴ In the majority of applications, the resonators' most important characteristics are the Q -factor and their temperature stability. In order to be useful for ESR, however, a resonator must also provide a high microwave magnetic field at the volume where the sample is placed, preferably with a low electric-field component at the same spot. In addition, it should enable variable coupling capabilities, since each sample may have its own dielectric

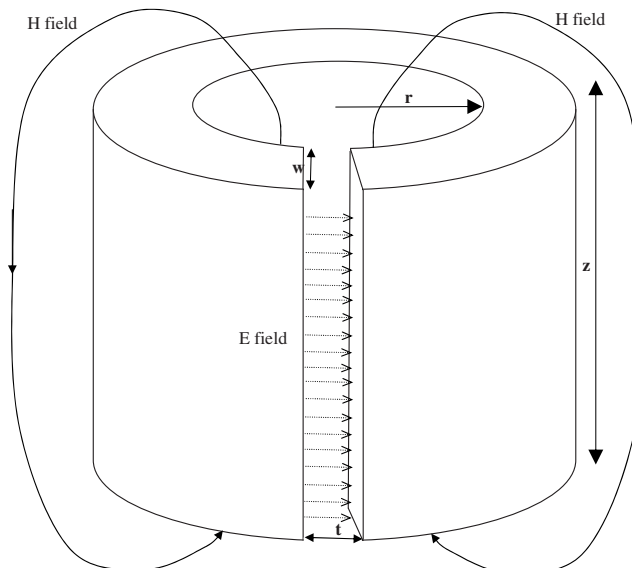


FIG. 1. Typical conventional metallic loop-gap resonator.

properties and thus affect the properties of the resonator and the coupling. The planar ESR resonators described in the literature^{19-21,25-27} are based on these notions. For example, some designs employ either straight or curved self-resonant half-wavelength (λ) microstrip transmission lines.^{20,21} Other designs use smaller microstrip-based structures that are made resonant by the addition of an appropriately shaped printed tuning stub with distributed capacitance.¹⁹ As noted above, all these structures have *fixed* coupling mechanisms based on a microstrip transmission line with a certain fixed resonator-line distance gap, and often also with some matching and tuning stubs leading to the resonator. As already explained, these stub components, especially those for tuning, significantly increase the resonators' effective volume.

A possible solution around this problem, considered in this work, is to begin from the concept of loop-gap resonators and "shrink" their height down to the point that they become surface resonators. Loop-gap resonators have been known for many years in the context of ESR.²⁸ These structures, schematically depicted in Fig. 1, are based on an inductive open loop, terminated by a capacitive gap between the loop's open ends. These self-resonant structures are very efficient due to the microwave magnetic field being well inside the loop. Furthermore, they can be coupled to by a wide variety of variable coupling mechanisms, such as loop antennae and microstrip lines. However, all loop-gap resonator designs mentioned in the literature have a rather large z dimension. This is due to the required large capacitance for the resonator's "gap" and the linear dependence between the said capacitance and z . Further insight into this problem can be gained by examining the following expressions for resonance frequency of loop-gap resonators.

The resonance frequency, ν , of loop-gap resonators, such as the one shown in Fig. 1, can be estimated through the expressions²⁹

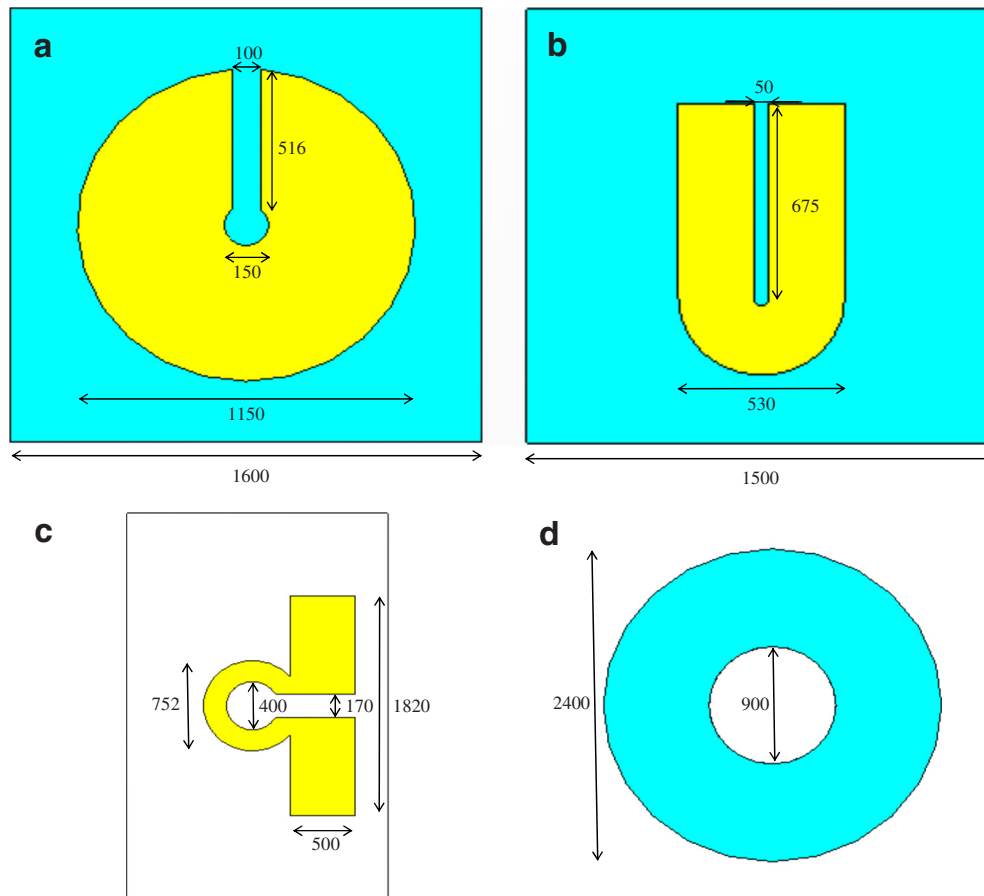


FIG. 2. (Color online) Physical dimensions of the (a) LGR150, (b) LGR50, (c) omega-type, and (d) rutile resonators. All dimensions are in microns.

$$L \approx \frac{\mu_0 \pi r^2}{z + 0.9r}, \quad C \approx \frac{\varepsilon_r \varepsilon_0 (w + t)(z + t)}{t}, \quad (6)$$

$$\nu = \frac{1}{\sqrt{2\pi LC}}. \quad (7)$$

Here, μ_0 is the free-space permeability, ε_r is the dielectric constant of the filler material in the gap, and ε_0 is the free-space permittivity. For $\nu=15$ GHz, typical dimensions of a small resonator used for conventional ESR spectroscopy may be $r=0.62$ mm, $z=3.5$ mm, $w=0.35$ mm, and $t=0.04$ mm (with no dielectric material in the gap). Starting from these values, let us see what happens if one wishes to produce a surface loop-gap microresonator. First, the radius, r , must be decreased and also the height, z , should shrink to the micron range. According to Eq. (6) this would result in a decrease in loop inductance but mainly in a sharp reduction of the “gap” capacitance, both of which would boost the resonance frequency to an unwanted regime. In order to compensate for these necessary geometrical changes, two design modifications are made to regain gap capacitance: (a) the surface resonator is applied to a substrate with high permittivity (large ε_r) and (b) the width, w , is increased. Equation (6) is valid only under some limiting geometrical assumptions and shrinking the height of the resonator makes it quite inaccurate. Still, our assumption was that it can be used to provide a preliminary estimate for the required resonator dimensions, which must then be further optimized using a full finite-

element microwave simulation (CST microwave studio in our case). Our current design work included two types of surface loop-gap microresonators:

- (a) LGR150. The resonator’s design and dimensions are shown in Fig. 2(a). It is made of a $0.3 \mu\text{m}$ gold layer deposited on a $1.6 \times 1.6 \times 0.22 \text{ mm}^3$ single-crystal rutile substrate *with no ground plane on the bottom side*. Rutile (TiO_2) has an anisotropic crystal structure, leading to anisotropic permittivity of ~ 165 along the crystal’s C-axis and ~ 85 along the other two axes (at room temperature).³⁰ In this design, the crystal’s C-axis is in the resonator’s plane, perpendicular to the gap’s long axis. The structure’s resonance frequency, calculated by Eq. (7), is 23.2 GHz (assuming that the permittivity in the gap is 165). Capacitance is probably underestimated by Eq. (6) and certainly other distributed effects exist, leading to the more accurate finite-elements calculation result of a resonance frequency of 12.36 GHz. The calculated microwave magnetic- and electric-field distributions of this resonator are shown in Fig. 3(a). A clear resonance mode is apparent with the microwave magnetic field centered in the “loop” area and the microwave electric-field located mainly in the “gap” area. However, in contrast with conventional loop-gap resonators, there is quite a large variation in the magnetic and electric-fields along the “gap.” This is because w is much larger (in proportion to r) than in

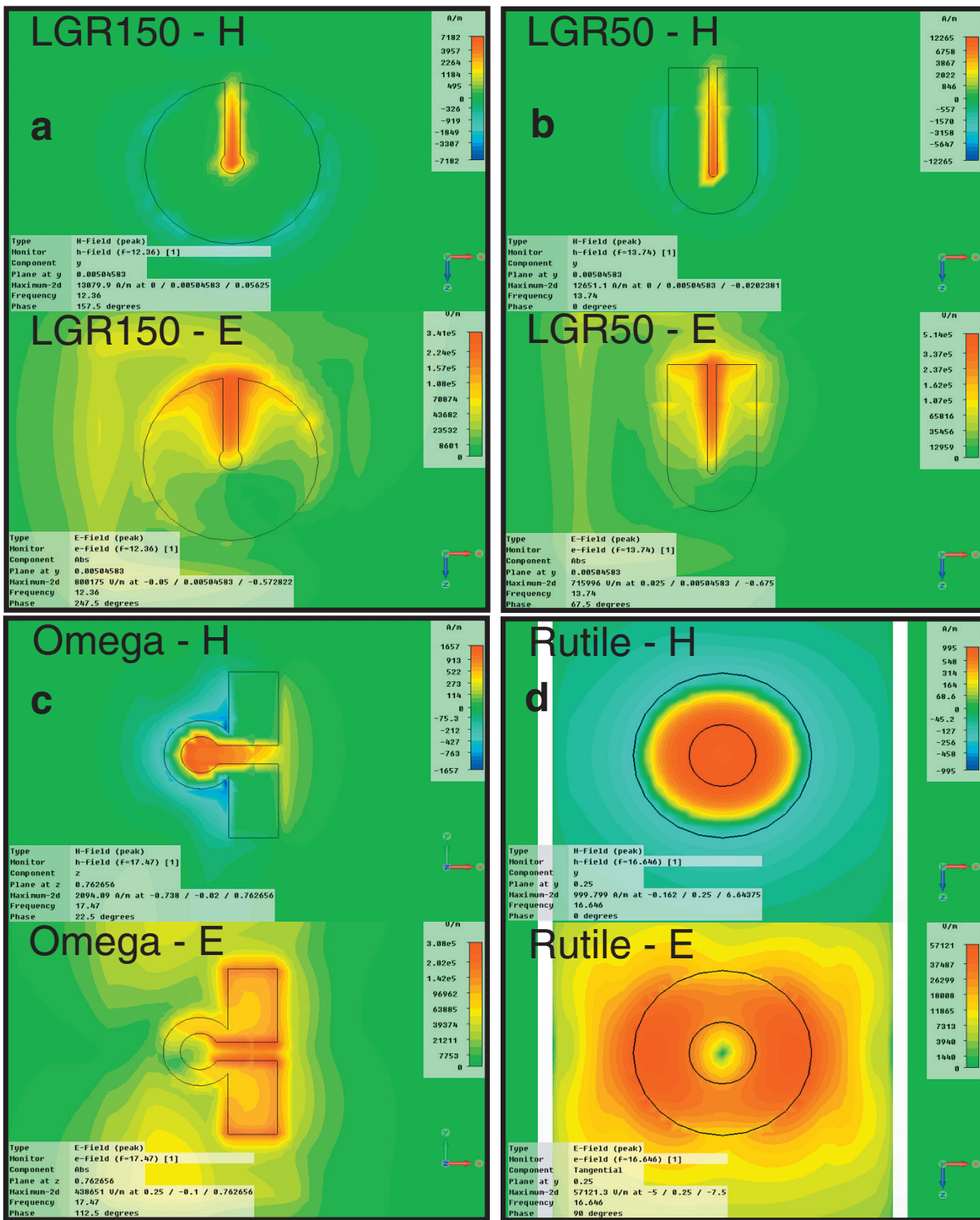


FIG. 3. (Color) Magnetic (marked as H) and electric (marked as E) fields, as calculated by the finite-element microwave simulation, for the (a) LGR150, (b) LGR50, (c) omega, and (d) rutile resonators. Fields are plotted for a plane that is located $5 \mu\text{m}$ above the surface of the resonators ($5 \mu\text{m}$ above the upper side of the ring of the rutile resonator). This is assumed to be the distance of closest approach for a flat sample positioned on the resonators. The incident microwave power is 1 W for all resonators.

common loop-gap configurations, a fact that gives it a distributed “flavor” in addition to its lumped role. One might also consider this kind of structure as a “hybridization” of loop-gap with slot-line resonators.

- (b) LGR50. This resonator’s design and dimensions are shown in Fig. 2(b). It is the “little brother” of the LGR150, also made of a $0.3 \mu\text{m}$ gold layer deposited

on a $1.5 \times 1.5 \times 0.22 \text{ mm}^3$ single-crystal rutile substrate with no ground plane on the bottom side. In this design, the crystal’s C-axis is in the rutile plane, parallel to the gap’s long axis. The resonance frequency of this structure calculated by the finite-elements software is 13.74 GHz. The calculated microwave magnetic- and electric-fields distributions are shown in Fig. 3(b),

which presents a clear resonance mode whose microwave field behavior is similar to that of the LGR150. The distributed nature of the “gap” area, as described above, is even more pronounced here than in the LGR150 configuration. In addition to these new structures, we analyzed the properties of two more familiar devices: a surface omega-type resonator and a ring dielectric resonator.

- (c) Omega. The resonator’s design and dimensions are shown in Fig. 2(c). It is based on the design presented in Ref. 20. Our omega resonator is made of Rogers RT/doroid 6010LM microwave substrate with permittivity of 10.2 and thickness of $625\ \mu\text{m}$. The substrate has two $35\ \mu\text{m}$ copper layers deposited on its upper and bottom sides. The omega resonator is on the upper side with the ground plane layer *remaining* on the bottom side. The resonance frequency of this structure is the one in which the entire length of this curved microstrip transmission line structure is $\sim\lambda/2$. For 17 GHz this corresponds to $\sim 3250\ \mu\text{m}$ (for the substrate and line parameters given above). Actual finite-element calculations found a resonance frequency of 17.46. The calculated microwave magnetic- and electric-field distributions are shown in Fig. 3(c). A resonance mode is apparent with the microwave magnetic field centered in the “loop” area and the microwave electric-field located along the conductor edges.
- (d) Rutile. Another, more common, small resonator is the single ring dielectric resonator.^{31–33} It is not of the surface type, but still has a rather small V_c compared to rectangular metallic cavities, for example. In this work we use for comparison a resonator made of single-crystal rutile. The resonator’s design and its dimensions are shown in Fig. 2(d). The rutile’s C-axis is in the ring plane (along the x-axis). The resonator has a thickness (height) of $500\ \mu\text{m}$ and is located in a metal cylindrical shield with an inner diameter of 4.6 mm (the previous three resonators were modeled without any shield). The resonance frequency was calculated by finite-element simulation and found to be 16.65 GHz. The microwave magnetic- and electric-field distributions are shown in Fig. 3(d). A resonance mode (known as $\text{TE}_{01\delta}$ in the context of dielectric resonators)³³ is apparent with the microwave magnetic field maximum at the center of the ring and the electric-field maximal around the ring. The mode has no complete cylindrical symmetry due to the anisotropic permittivity of the single-crystal rutile.

Let us now consider more carefully some of the differences between these four configurations. The intention of these resonators is to provide high sensitivity for the measurement of small, often flat samples. We have shown that sensitivity increases as V_c decreases [Eq. (5)]; therefore, it is important to look not only at the distribution of the 2D fields shown in Fig. 3, but also at the spatial dependence of fields on the distance from the resonator surface. This dependence is shown in Fig. 4 for the location of the maximum magnetic field (i.e., at the center of the resonators). The small surface

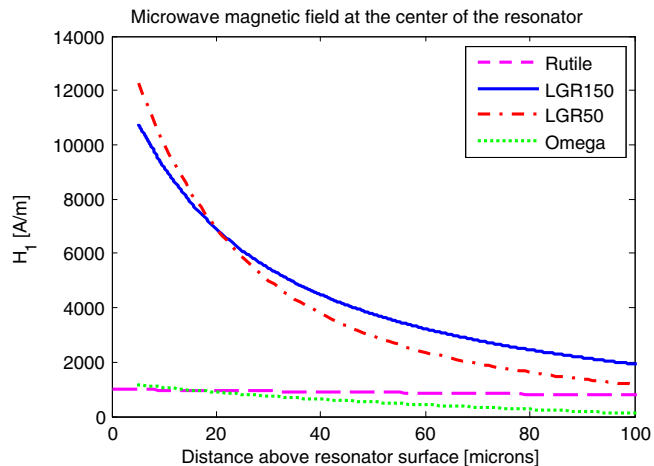


FIG. 4. (Color online) Microwave magnetic field for the (a) LGR150, (b) LGR50, (c) omega, and (d) rutile resonators, as a function of the distance from the surface of the resonators (distance from the upper side of the rutile resonator). The fields are plotted for the strongest field point in the resonator plane (about the center of the loop for each resonator).

resonators have a very steep field dependence on height, with the field falling to 50% of its maximal value after ~ 20 and $\sim 30\ \mu\text{m}$ for the LGR50 and LGR150 configurations, respectively. The fields in the omega resonator fall to 50% of their maximal value after $\sim 42\ \mu\text{m}$, while the fields from the Rutile dielectric resonator change by only $\sim 20\%$ in the first $100\ \mu\text{m}$ above the resonator’s surface.

Following the description of the resonance modes of the four configurations above, we now consider the coupling method. The coupling method for resonators used for ESR measurements should be adjustable. This enables accounting for the varying properties of the resonator when different samples are inserted into it, or when its properties change at different temperatures. In addition, coupling should not interfere with sample positioning. This means that in our surface resonators, for which the samples are placed on their upper (metallic) part, the coupling mechanism should approach the resonators from the bottom (i.e. the side with the dielectric layer). The coupling methods chosen in view of all these considerations are shown in Fig. 5. For the LGR150, LGR50, and omega resonators, a $550\ \mu\text{m}$ wide standard microstrip line on a $254\ \mu\text{m}$ thick substrate with $\epsilon=3.5$ was

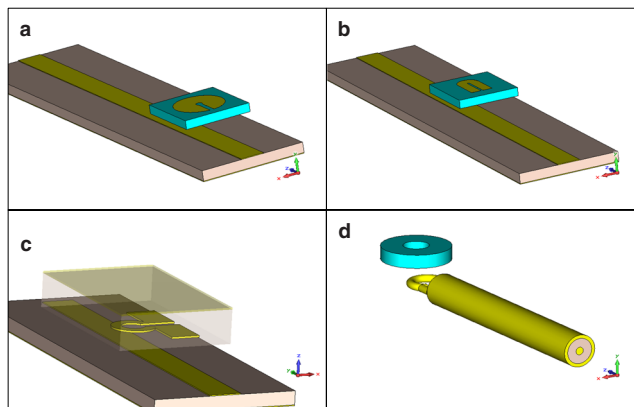


FIG. 5. (Color online) A mechanical drawing showing the coupling method to the (a) LGR150, (b) LGR50, (c) omega, and (d) rutile resonators.

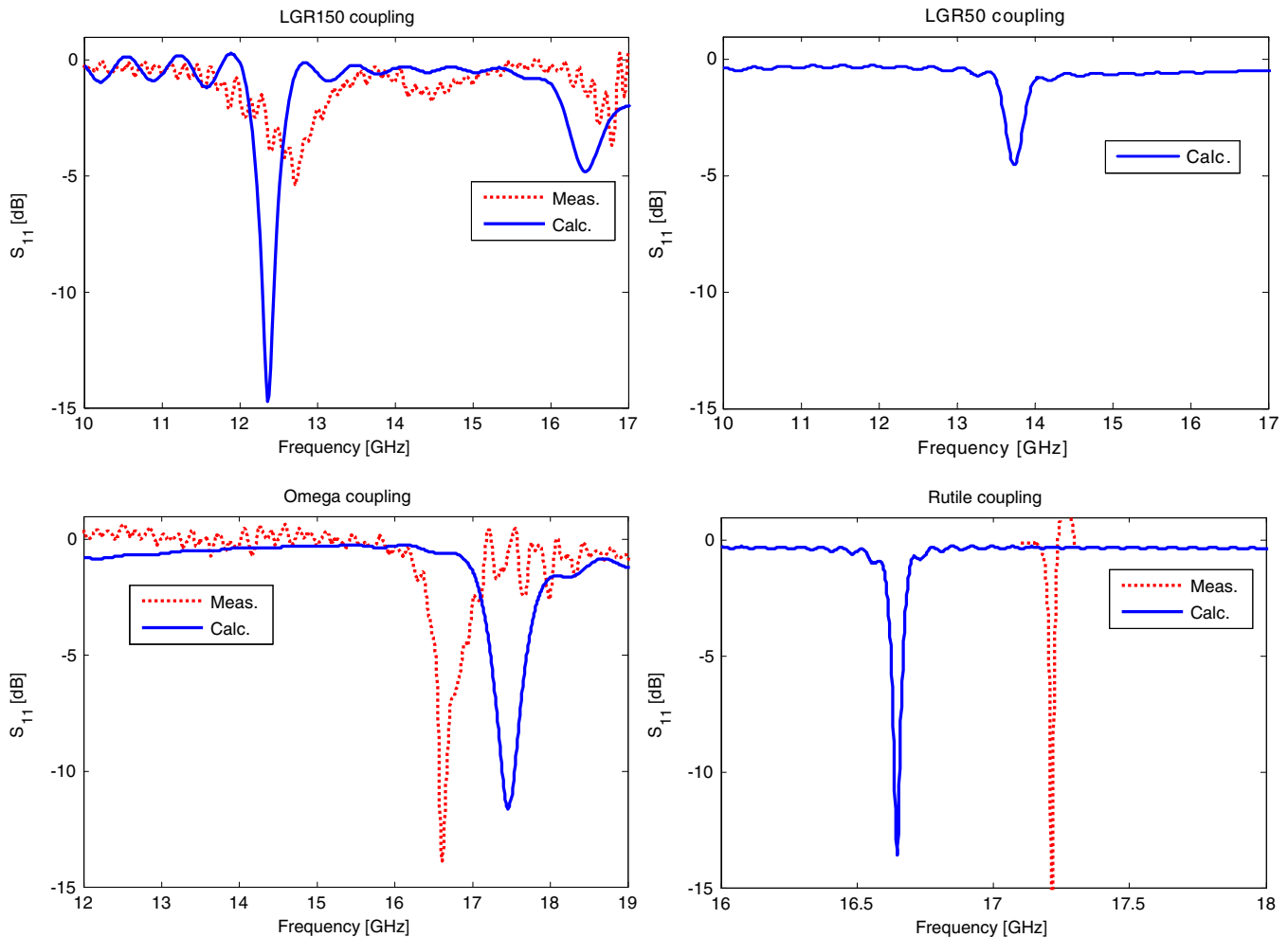


FIG. 6. (Color online) Calculated and measured S_{11} parameters as a function of the incident microwave frequency for the (a) LGR150, (b) LGR50, (c) omega, and (d) rutile resonators. The graphs represent the optimal coupling geometry that was found via calculation and during experimental measurements.

used. Coupling in the LGR50 and the LGR150 models is done via the E-field component, as shown in Figs. 5(a) and 5(b), while in the omega resonator it is done through the H-field component. In the case of the LGR50 and 150 resonators, the small thickness of the substrate enables coupling from the back, leaving an open space on top of the resonator for the sample. Coupling can be altered by changing the position of the line with respect to the resonator. This is achieved by placing the microstrip line on manually movable XY linear stages (not shown in Fig. 5). In the case of the omega resonator, the ground plane prevents coupling from the back and the microstrip line must be placed above the resonator. However, the line does not have to be in close proximity to the omega resonator to achieve sufficient coupling, leaving some space available in between for the sample (whereas in the case of the LGR150 and LGR5 the line must be very close to the substrate back to enable sufficient coupling). As noted above, the relative position of the resonator with respect to the microstrip line changes the coupling properties and enables matching the resonator to the line when different samples are positioned on it (or between the line and the resonator in the case of the omega-type device). Variable coupling in the rutile resonator is shown in Fig. 5(d) and is achieved by means of a semirigid coaxial line

with its center lead exposed and soldered to the shield conductor. This generates a magnetic loop that can be coupled via the H-field component to the resonator. As in the case of microstrip coupling, the relative position of the resonator with respect to the coaxial loop (adjusted by movable XY linear stages) changes the coupling properties. The calculated coupling properties (S_{11} parameters versus frequency) for the four resonator structures are given in Fig. 6 (blue lines).

The summary of calculated parameters for the four resonators presented above is provided in Table I. They will later be compared to the experimental data that also appear in the same table. Table I also lists the properties of a commercial Bruker miniature split-ring resonator (MS-2) for reference purposes.

IV. EXPERIMENTAL METHODS

Following these design processes, the four configurations described above were manufactured and their properties measured. The surface loop-gap microresonators were manufactured out of a 220 μm thick, 10×10 mm² piece of rutile single-crystal (MTI Corporation, CA, USA) with 110 orientation (the C-axis is in the crystal surface plane). The details of this photolithographic procedure appear in Table II.

TABLE I. Summary of calculated and measured properties of the four resonators considered in this work.

Resonator type	f_0^{calc} (GHz)	f_0^{meas} (GHz)	Q^{calc}	Q^{meas}	V_c (mm ³) ^a	P_{MW} at max. sig. ^b (W)	C_p^{calc} (gauss/ $\sqrt{\text{W}}$)	C_p^{meas} (gauss/ $\sqrt{\text{W}}$) ^c	Spin sensitivity (calc. for LiPc) ^d (spins/ $\sqrt{\text{Hz}}$)	Spin sensitivity (calc. for E' in SiO ₂) ^e (spins/ $\sqrt{\text{Hz}}$)	Spin sensitivity (meas. for E' in SiO ₂) ^f (spins/ $\sqrt{\text{Hz}}$)
LGR150	12.36	12.72	28	15	0.0025	12×10^{-3}	164	86	$1.9 \times 10^7 / 1.1 \times 10^7$	$2.5 \times 10^8 / 1.5 \times 10^8$	$3.1 \times 10^8 / 1.8 \times 10^8$
LGR50	13.74	...	68	...	0.0012	...	159	...	$7.1 \times 10^6 / 5.2 \times 10^6$	$9.5 \times 10^7 / 7.0 \times 10^7$...
Omega	17.46	16.61	25	30	0.0360	340×10^{-3}	14.7	15	4.5×10^7	5.9×10^8	3×10^8
Rutile	16.65	17.21	260	530	2.32	45×10^{-3}	12.5	14	8.4×10^7	1.1×10^9	4.5×10^8
MS-2 ^g	...	9.5	...	24	18.8	...	1.2	1	$3.7 \times 10^9 / 1.5 \times 10^9$	$1.4 \times 10^{11} / 5.8 \times 10^{10}$...

^a V_c is calculated based on the filling factor of a pointlike volume element V_v (with a volume of $1 \mu\text{m}^3$) located at the maximum field just above the resonator ($5 \mu\text{m}$ above the surface). For the Rutile resonator, the point is $5 \mu\text{m}$ above the upper side of the ring. If V_c is calculated based on the field at the center of the Rutile resonator, it is found to be $\sim 1.3 \text{ mm}^3$.

^bThe measured microwave power going into the resonator at maximum ESR signal for the Hahn echo sequence with 90° and 180° pulse durations of 35 and 70 ns, respectively.

^cSee the text in the discussion section explaining the method for calculating C_p from the measured P_{MW} values.

^dThe calculation assumes $T_2^* = 2.5 \mu\text{s}$ and $T_1 = 3.5 \mu\text{s}$ (Ref. 37). The numbers in bold font are calculations assuming a resonance frequency of 17 GHz. The numbers in regular font are calculations carried out for the actual resonance frequency of the resonator (only in case it is much lower than 17 GHz).

^eThe calculation assumes $T_2^* = 0.1 \mu\text{s}$ and $T_1 = 200 \mu\text{s}$ (Ref. 38). The numbers in bold font are calculations assuming a resonance frequency of 17 GHz. The numbers in regular font are calculations carried out for the actual resonance frequency of the resonator (only in case it is much lower than 17 GHz).

^fSee the text in the discussion section explaining the method for measuring spin sensitivity. In the case of the LGR150 resonator, which operates at relatively low resonance frequency, we report both the actual measured spin sensitivity (at 12.72 GHz, in regular font) and the projected spin sensitivity at 17 GHz (in bold font).

^gThis is a standard split-ring pulsed ESR resonator, available from Bruker, 2 mm in diameter and 6 mm long. Data are based on Ref. 39.

Following preparation, the individual resonators were cut from the large piece by means of a diamond wire saw.

The omega resonator was manufactured using standard microwave circuit board production methods, based on the geometry shown in Fig. 2(c) (outsourced to Cidav Ltd., Israel). The rutile resonator was produced in our laboratory out of a $500 \mu\text{m}$ thick, $10 \times 10 \text{ mm}^2$ piece of rutile single-crystal, similar to the one described above. It was first sliced to $\sim 2.5 \times 2.5 \text{ mm}^2$ square pieces using a diamond wire saw and then drilled at the center using a diamond driller. The squares with the hole were then grinded to their required diameter by means of a conventional grinding-stone procedure.

TABLE II. Preparation protocol for surface loop-gap microresonators (LGR50 and LGR150).

Surface	Wafer type: TiO ₂
Preparation	Cleaning: Ultrasonic bath in acetone, methanol, and isopropanol (5 min each). Final rinse with water. Heating: on plate at 300°C for 10 min
Photoresist coating	Photoresist type: Clariant AZ 5214 E Spin velocity: 1500 rpm Spin time: 1 min
Prebake	On a hotplate at 110°C for 1.3 min
Exposure	System: Karl Suss MA-6 mask aligner Exp. type: Soft contact Alignment gap: start with $35 \mu\text{m}$ and eventually bring to full contact Exp. time: 1.9 s
Postbake	On a hotplate at 120°C for 2 min.
Flat exposure	Exposure without mask on mask aligner for 15 s
Development	Total development time: 40 s
Metal deposition	System: Temescal FC-1800 E-beam evaporator First layer: Ti(50 A deg) Second layer: Au(3000 A deg)
Lift-off	Ultrasonic bath in acetone for 5 min

Following manufacture, the resonators were placed on a mechanical fixture near the microwave feed lines, which were then connected to linear variable XY stages. The microwave lines were connected to a vector network analyzer (Agilent E8361A) which measured the resonators' S_{11} parameters (for optimal coupling properties). The resulting measurements are shown in Fig. 6 (red lines). Sufficient coupling was obtained in all configurations, in good agreement with the theory, except for the LGR50. The latter model showed reasonable coupling when the microstrip line was attached to the front of the resonator, but coupling from the back was too weak to be measured reliably. Coupling to the rutile resonator, which has a much higher Q -factor than the surface resonators, was much easier and conformed well to the theoretical predictions. The measured resonance frequency and the Q -factor of the three resonators that showed good coupling are listed in Table I.

V. PULSED ESR EXPERIMENTAL RESULTS

The next stage was to acquire ESR signals for all resonator configurations using a test sample with a well-known spin concentration. The experiments were carried out on our home-made pulsed ESR system.⁹ The chosen test sample was a $100 \mu\text{m}$ thick SiO₂ slide irradiated by γ -irradiation from a ^{60}Co source (carried out at the "Nahal Sorek" facility, Yavneh, Israel). This produced a rather homogenous distribution of the so-called E' paramagnetic center defects in the slide.^{16,34} The sample spin concentration was found to be $\sim 3 \times 10^{15}$ spins/cm³ by comparing its double integral CW ESR signal to that of a $1 \mu\text{M}$ trityl solution in a capillary tube (both measured under the same condition in a commercial Bruker EMX X-band CW ESR system). During measurements, the sample was placed just above the surface loop-gap microresonator (LGR150 only, since we could not couple well to the LG50 resonator from the back, as noted

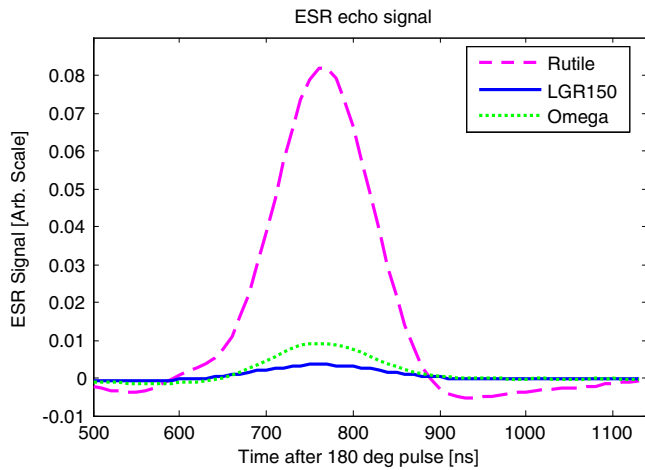


FIG. 7. (Color online) The ESR echo signal of the γ -irradiated SiO_2 test sample, as measured by the LGR150, omega, and rutile resonators (Ref. 40).

above). As for the omega-type resonator, the sample was placed between the coupling line and the resonator. In the case of the rutile resonator, it was placed just above the dielectric ring.

The measured ESR echo signals acquired by the three resonators for which effective coupling were achieved are shown in Fig. 7. A standard two-pulse Hahn echo sequence was used with 90° and 180° pulse durations of 35 and 70 ns, respectively. Similar measurements were carried out at field offset of 100 gauss from resonance in order to record the noise levels (results not shown). During these measurements we also recorded the power required for achieving the maximum ESR signal and translated that data into the measured C_p value (see Table I and the discussion section below for more details). Furthermore, the measured ESR signal-to-noise-ratio, along with our knowledge of the sample's spin concentration and its dimensions, were used to obtain the spin sensitivity for the different resonators (see Table I and the discussion section below for more details).

VI. DISCUSSION

First, let us consider the quality of the performed calculations compared to the experimental observation, as depicted in Table I. The measured f_0 values are in good agreement with the theoretical predictions for all three resonators. Variations of up to 5% between theoretical and measured resonant frequencies are not unexpected given the micron tolerances in the design. As for the calculation of the Q -factor, it seems that the finite-element model is less accurate but still good enough to show important trends, providing for example a relatively high Q -factor for the rutile resonator and low values for the surface resonators. The next calculated parameter of importance is V_c , which is derived from the calculated magnetic fields in the resonator (see Figs. 3 and 4 and the definition of V_c above). The resonators' magnetic fields cannot be measured directly, and thus it is hard to "measure" V_c , but this parameter comes into play in the measured power-to-field conversion factor, C_p , and in spin sensitivity. These are the most important "bottom line" parameters that characterize resonator performance. How-

ever, their extraction from the experimental data is not trivial and requires some discussion. Let us now see how the experimental results should be understood with respect to these two parameters.

From a first glance at Fig. 7 it seems that the rutile resonator is the most sensitive one. However, this is because it is the largest of all three devices, leading to the measurement of a relatively large sample volume, which is not a direct measure of its spin sensitivity. The absolute spin sensitivity, as depicted by Eq. (5), relates to the minimal number of spins that can be measured when they are placed at the most sensitive point in the resonator (where B_1 is the largest). In order to extract spin sensitivity from the measured ESR signal, one must know the effective number of spins that were measured by the resonator. If the microwave B_1 field in the sample volume was homogenous, then it would have been clear that the ESR signal originates from a known number of spins (based on the sample volume and its spin concentration), and the measured ESR spin sensitivity could have been easily obtained. In practice, however, the fields in our resonators are highly inhomogeneous. Thus, in order to extract spin sensitivity out of the measured signal, one has to consider the 3D spatial dependence of the microwave magnetic fields and obtain from it the actual number of spins contributing to the signal.

The signal of our test sample can be calculated from Eq. (1), by summing up (integrating) the contributions from all individual small volume elements V_v in the sample. Clearly, due to the B_1 inhomogeneity, not all parts in the sample will contribute the same amount of signal, and therefore this integration should be done with attention to details. In Eq. (1) there are two places in which B_1 inhomogeneity comes into play. The first place is C_p , which is easy to take into consideration because it is simply the B_1 field for 1 W of input power at the locations of V_v used in signal integration. The second place is in the calculation of M , which is the measure of the specific magnetization in the laboratory xy plane contributing to the signal. For an echo signal, excited by non-ideal pulses with turning angles of θ and 2θ (which ideally should be the "90°" and "180°" pulses, respectively), magnetization in the laboratory xy plane will be proportional to^{16,35}

$$M = M_{\max} \sin^3(\theta). \quad (8)$$

Equation (8) assumes that the full ESR spectrum is excited by the MW pulses (valid for the irradiated SiO_2 sample employed in the experiments). The optimal turning angle θ is of course 90° but, since the fields are very inhomogeneous, most points in the sample will experience a nonoptimal turning angle during the experiment. In order to account for these issues we have performed a numerical calculation of the ESR signal with Eqs. (1) and (8), based on the calculated B_1 fields throughout the sample volume. The calculation was repeated several times with the turning angle θ in the most sensitive point of the resonator (having the largest C_p) serving as an experimentally variable parameter (related to the power of the microwave pulses). This repeated procedure mimics the experimental setup where we increased the power up to the level in which the best ESR signal was obtained. This opti-

mal calculated value of the ESR signal is denoted S^{opt} . It was found that turning angles of $\theta \sim 288^\circ$ and $\theta \sim 272^\circ$ (at the point of largest B_1) provided the optimal signals for the LGR150 and omega resonators, respectively. As for the rutile resonator, a turning angle of $\theta \sim 94^\circ$ was found to be optimal. The measured C_p values that appear in Table I are based on these simulations and the measured power that were found to provide the optimal ESR signal.

Another type of ESR signal, which is hypothetical, can be calculated assuming that all spins in the sample are concentrated in the resonator's most sensitive volume element, V_v (denoted S^{max}). The ratio between the two ($S^{\text{opt}}/S^{\text{max}}$), multiplied by the total number of spins in the sample, provides us with the effective number of spins actually contributing to the signal. This number of effective spins is smaller than the actual number of spins in the sample since it assumes that all of these "effective spins" were at the point of largest B_1 . The number of effective spins contributing to the signal is used to obtain the resonator's experimental spin sensitivity. Furthermore, since the LGR150 and LGR50 resonators were designed and operated at lower frequencies than the omega and the rutile devices, Table I lists also the "adjusted" spin sensitivity of these resonators, assuming they were operated at 17 GHz. These adjustments for the calculated and the experimental spin sensitivity values are based on Eq. (5). Agreement between the calculated and experimental spin sensitivity values is fair. For the LGR150 resonator, the experimental sensitivity value is a little worse than the calculated one, while for the omega and the rutile resonators, it is a little better. The more favorable sensitivity in the latter two cases can be due to overestimation of system losses [the factor of 4 in Eq. (1)], and also due to the higher Q factor measured versus the calculated one for the rutile device (the CST simulation tends to underestimate Q for high Q structures). The less favorable experimental sensitivity found for the LGR150 model falls within reasonable production and field calculation errors that can lead to such small variations.

To conclude this section, it is evident from Table I that the experimental results are in fair agreement with the theoretical predictions. These results show that for a γ -irradiated SiO_2 sample, which is not optimal for high spin sensitivity (due to its relatively long T_1 and short T_2^*), one can expect to achieve spin sensitivity of slightly more than 10^6 spins per 1 h of acquisition time (which improves sensitivity by a factor of $\sqrt{3600}=60$). These numbers apply to the LGR150 model and especially to the LGR50 device, in which coupling was achieved only from the top side, but may be still useful for some types of samples. The importance of reducing the resonator's volume in order to increase its C_p and the absolute spin sensitivity is apparent from our results, especially when these are compared to those achievable with one of the smallest commercial resonator (the Bruker MS-2). Spin sensitivity can be improved by more than one order of magnitude, to $\sim 10^5$ spins per 1 h of acquisition time, for the more favorable LiPc sample.

The measurements and calculations presented here are all only for room temperature conditions. This implies that if we consider a LiPc sample with 10^5 spins, only ~ 129 spins

are actually contributing to the signal (due to the Boltzmann factor). In practice, at such small number of spins, the statistical polarization³⁶ becomes the dominant contributor to the signal (contributing $\sqrt{10^5} \sim 316$ spins). Since this polarization can be averaged with a repetition rate that is faster than $1/T_1$ without loss of signal, this opens up interesting opportunities for increasing spin sensitivity further. Additional improvements in sensitivity may also be achieved in the future by working with higher magnetic fields, and especially by working with low cryogenic temperatures, in which the resonators' quality factor can be improved by a factor ranging from ~ 10 (for gold deposition) up to $\sim 10\,000$ (for resonators made of a thin superconducting layer). A higher quality factor should also make it easier to efficiently couple to even smaller structures. cw ESR can greatly benefit from such high Q -values. However, for pulsed ESR, such high Q can only be useful for samples having very narrow lines and very long relaxation times (due to bandwidth and resonator "dead time" issues).

ACKNOWLEDGMENTS

This work was partially supported by Grant No. 213/09 from the Israeli Science Foundation, Grant No. 201665 from the European Research Council (ERC), and by the Russell Berrie Nanotechnology Institute at the Technion. The help and support of Arkady Gavrilov and Avshalom Shai from the Technion's Micro-Nano Fabrication Unit are greatly appreciated

- ¹ See <http://www.bruker-biospin.com/cwperformance-sense.html>. The conditions of these measurements are room temperature, X-band frequency, for narrow line samples of ~ 1 gauss that do not saturate.
- ² C. L. Degen, M. Poggio, H. J. Mamin, C. T. Rettner, and D. Rugar, *Proc. Natl. Acad. Sci. U.S.A.* **106**, 1313 (2009).
- ³ D. Rugar, R. Budakian, H. J. Mamin, and B. W. Chui, *Nature (London)* **430**, 329 (2004).
- ⁴ C. Durkan and M. E. Welland, *Appl. Phys. Lett.* **80**, 458 (2002).
- ⁵ M. Mannini, P. Messina, L. Sorace, L. Gorini, M. Fabrizio, A. Caneschi, Y. Manassen, P. Sigalotti, P. Pittana, and D. Gatteschi, *Inorg. Chim. Acta* **360**, 3837 (2007).
- ⁶ Y. Manassen, R. J. Hamers, J. E. Demuth, and A. J. Castellano, *Phys. Rev. Lett.* **62**, 2531 (1989).
- ⁷ G. Balasubramanian, I. Y. Chan, R. Kolesov, M. Al-Hmoud, J. Tisler, C. Shin, C. Kim, A. Wojcik, P. R. Hemmer, A. Krueger, T. Hanke, A. Leitenstorfer, R. Bratschitsch, F. Jelezko, and J. Wrachtrup, *Nature (London)* **455**, 648 (2008).
- ⁸ J. M. Taylor, P. Cappellaro, L. Childress, L. Jiang, D. Budker, P. R. Hemmer, A. Yacoby, R. Walsworth, and M. D. Lukin, *Nat. Phys.* **4**, 810 (2008).
- ⁹ A. Blank, E. Suhovoy, R. Halevy, L. Shtirberg, and W. Harneit, *Phys. Chem. Chem. Phys.* **11**, 6689 (2009).
- ¹⁰ K. Lips, P. Kanschhat, and W. Fuhs, *Sol. Energy Mater.* **78**, 513 (2003).
- ¹¹ P. Pichler, *Intrinsic Point Defects, Impurities, and Their Diffusion in Silicon* (Springer, Wien, New York, 2004).
- ¹² M. Mannini, D. Rovai, L. Sorace, A. Perl, B. J. Ravoo, D. N. Reinhoudt, and A. Caneschi, *Inorg. Chim. Acta* **361**, 3525 (2008).
- ¹³ P. P. Borbat, A. J. Costa-Filho, K. A. Earle, J. K. Moscicki, and J. H. Freed, *Science* **291**, 266 (2001).
- ¹⁴ A. Blank, C. R. Dunnam, P. P. Borbat, and J. H. Freed, *J. Magn. Reson.* **165**, 116 (2003).
- ¹⁵ A. Blank and J. H. Freed, *Isr. J. Chem.* **46**, 423 (2006).
- ¹⁶ G. A. Rinard, R. W. Quine, R. T. Song, G. R. Eaton, and S. S. Eaton, *J. Magn. Reson.* **140**, 69 (1999).
- ¹⁷ C. P. Poole, *Electron Spin Resonance: A Comprehensive Treatise on Experimental Techniques* (Wiley, New York, 1983).
- ¹⁸ M. T. Sebastian, *Dielectric Materials for Wireless Communication*

- (Elsevier, Amsterdam, Boston, 2008).
- ¹⁹R. Narkowicz, D. Suter, and I. Niemeyer, *Rev. Sci. Instrum.* **79**, 084702 (2008).
- ²⁰R. Narkowicz, D. Suter, and R. Stonies, *J. Magn. Reson.* **175**, 275 (2005).
- ²¹A. C. Torrezan, T. P. Mayer Alegre, and G. Medeiros-Ribeiro, *Rev. Sci. Instrum.* **80**, 075111 (2009).
- ²²J.-S. Hong and M. J. Lancaster, *Microstrip Filters for RF/Microwave Applications* (Wiley, New York, 2001).
- ²³Y. T. Lee, J. S. Lim, C. S. Kim, D. Ahn, and S. Nam, *IEEE Microw. Wirel. Compon. Lett.* **12**, 375 (2002).
- ²⁴J. Garcia-Garcia, J. Bonache, I. Gil, F. Martin, M. D. Velazquez-Ahumada, and J. Martel, *IEEE Trans. Microwave Theory Tech.* **54**, 2628 (2006).
- ²⁵B. Johansson, S. Haraldso, L. Petterss, and O. Beckman, *Rev. Sci. Instrum.* **45**, 1445 (1974).
- ²⁶C. P. Lin, M. K. Bowman, and J. R. Norris, *J. Magn. Reson.* **65**, 369 (1985).
- ²⁷W. J. Wallace and R. H. Silsbee, *Rev. Sci. Instrum.* **62**, 1754 (1991).
- ²⁸J. S. Hyde and W. Froncisz, Proceedings of the National Electronics Conference, 1981.
- ²⁹S. S. Eaton, G. R. Eaton, and L. J. Berliner, *Biomedical EPR* (Kluwer Academic/Plenum, New York, 2004).
- ³⁰M. E. Tobar, J. Krupka, E. N. Ivanov, and R. A. Woode, *J. Appl. Phys.* **83**, 1604 (1998).
- ³¹M. Jaworski, A. Sienkiewicz, and C. P. Scholes, *J. Magn. Reson.* **124**, 87 (1997).
- ³²A. Blank, E. Stavitski, H. Levanon, and F. Gubaydullin, *Rev. Sci. Instrum.* **74**, 2853 (2003).
- ³³D. Kajfez and P. Guillon, *Dielectric Resonators* (Artech, Dedham, MA, 1986).
- ³⁴S. Agnello, R. Boscaino, G. Buscarino, and F. M. Gelardi, *J. Non-Cryst. Solids* **345–346**, 505 (2004).
- ³⁵A. Blank and H. Levanon, *Spectrochim. Acta, Part A* **58**, 1329 (2002).
- ³⁶H. J. Mamin, R. Budakian, B. W. Chui, and D. Rugar, *Phys. Rev. Lett.* **91**, 207604 (2003).
- ³⁷J. W. Stoner, D. Szymanski, S. S. Eaton, R. W. Quine, G. A. Rinard, and G. R. Eaton, *J. Magn. Reson.* **170**, 127 (2004).
- ³⁸G. R. Eaton, S. S. Eaton, R. W. Quine, D. Mitchell, V. Kathirvelu, and R. T. Weber, *J. Magn. Reson.* **205**, 109 (2010).
- ³⁹P. Höfer and P. Carl, Bruker Spin Report No. 157/158, 2006, p. 52.
- ⁴⁰C. Ebel, K. U. Ingold, J. Michon, and A. Rassat, *New J. Chem.* **9**, 479 (1985).